

A Compact Patch Antenna for 5G Communication (39 GHz-mmWave-n260) Employing Aperture Coupled Feeding Technique

Amit Abhishek

abhi.amit814@gmail.com

Birla Institute of Technology - Extension Centre Patna: Birla Institute of Technology - Patna Campus
<https://orcid.org/0000-0001-8287-9685>

Priyadarshi Suraj


Birla Institute of Technology - Extension Centre Patna: Birla Institute of Technology - Patna Campus

Research Article

Keywords: 5G, Aperture Coupled Feeding (ACF) Technique, Bandwidth (B.W), Higher frequency application, Microstrip patch antenna

Posted Date: July 27th, 2023

DOI: <https://doi.org/10.21203/rs.3.rs-2815364/v1>

License:  This work is licensed under a Creative Commons Attribution 4.0 International License.
[Read Full License](#)

Version of Record: A version of this preprint was published at Wireless Personal Communications on May 1st, 2024. See the published version at <https://doi.org/10.1007/s11277-024-11127-x>.

A Compact Patch Antenna for 5G Communication (39 GHz-mmWave-n260) Employing Aperture Coupled Feeding Technique

Amit Abhishek¹[0000-0001-8287-9685] and P. Suraj²

^{1,2} Department of ECE, Birla Institute of Technology, Mesra (Patna Campus), Patna-800014, India
¹abhi.amit814@gmail.com and ²psuraj@bitmesra.ac.in

Abstract. In the present work Aperture Coupled Feed (ACF) microstrip patch antenna for 5G communication is proposed. The proposed antenna has a very compact size of $2.2\lambda_g \times 2.2\lambda_g \times 0.3\lambda_g$ (mm³), it is printed on Rogers RT Duroid 5880 with $\epsilon_r = 2.2$. The antenna having two vertical layer of 0.8 mm separated by air gap of 0.035 mm. The upper edge of substrate has a circular ring patch working as radiator whereas bottom having no metallization. Upper portion of lower substrate has plus shape slot and at bottom is a rectangular feed line acting as feeder to patch antenna. The antenna operatable from 36.84 GHz to 46.78 GHz and having an operating frequency of 38.40 GHz. The overall B.W% achieved is 25.91% and peak gain observed to be 7.32 dB. The measured results are in close agreement with the simulated one. Prior to approaching ACF technique, a conventional microstrip patch antenna with circular radiator with size of $2.2\lambda_g \times 2.2\lambda_g \times 0.15\lambda_g$ (mm³), printed on single PCB of same material was considered. The antenna gets operatable from 33.07 GHz to 39.5 GHz and resonating at 38.02 GHz. The overall B.W% achieved is 17.10% and peak gain of 8.1 dB. Both antennas are good candidature for 5G Communications.

Keywords: 5G, Aperture Coupled Feeding (ACF) Technique, Bandwidth (B.W), Higher frequency application, Microstrip patch antenna

1 Introduction

Due to development in communication system, now 4G is getting replaces with 5G. As 5G have different advantages like better connectivity, lesser latency time, high data rate over 4G and it approaches by millimeter-wave (mm-wave) bands [1]. Wide band width with respective operating frequency Aperture coupled feed antenna is beneficial, also maintaining the compact size [2],[3]. This method is employed in satellite communication applications at the X-band, which encourages its applicability to 5G communication at the 39 GHz frequency [4]. As per the FCC different frequencies like 3.5 GHz, 6.2 GHz, 28 GHz, 38 GHz, 39 GHz and 47 GHz [5] are allotted for 5G communication. So, to develop patch antenna comparable with 5G, different researches have proposed their respective work, in [6], concave shaped patch surrounded by two mirror imaged C-shaped in MIMO configuration is suggested qualifying 28 & 38 GHz of frequency having gain of 7.46 and 8.56 dBi respectively. A reconfigurable 5G patch antenna having

switching capability between 28 GHz and 38 GHz using PIN diode is proposed [7]. Again in [8] a vertical stacked dipole antenna array capable of operating at 28 and 38 GHz with respective gain of 4.8 and 4.6 dBi is defined. [9,10] has proposed their work on 5G NRn78 band (3.3-3.8 GHz). In [8], hook shaped aperture coupled circularly polarized antenna having a B.W of 2.8 to 3.8 GHz with gain of 4.08 dBi is proposed. However, in [10] a dual polarized magneto-electric dipole with aperture coupled feed is proposed giving a B.W of 3.02 to 4.02 GHz with a gain ranging 7.9 to 8.5 dBi is proposed. In the continuous Air Filled SIW (AFSIW) technology is used and a better gain of 10.8 dBi response with 1×4 array for 26 and 28 GHz band has been achieved [11]. Air filled substrate integrated waveguide stacks having two layered PCB laminates and by removing the substrate locally and getting sidewalls by either edge plating [12] or rows of vias [13],[14], putting air-filled waveguides or cavities. [12],[15]-[19] AFSIW components along with antennas has been proposed for mm-Wave application. They are micro, low-cost and high-performance antennas, [20-22] with waveguide-fed and slot arrays [23],[24]. A rectangular array patch antenna using proximity coupling technique have been adopted satisfying B.W of 26.04 to 28.87 GHz [25]. Utilization of antenna at multiple places at certain angle these system gives vital role in usability and performance too. Either switching it to array for obtaining large gain substrate of graphene and polyethylene terephthalate shows good outcomes for proposing antennas [26-27]. Ka band (26.8-29.55 GHz) covers 5G band, antenna with SIW fed and resonator as a patch treat large gain and bandwidth efficiency [28]. For lower band application in 5G monopole antenna can be also a part for better performance. Ground element with different shapes or slots increases the antenna's performance in monopole technique [29-30]. Arraying into several numbers we can increase the parameters by employing some new feeding technique for better performance [31]. Through all the discussion above, we observe aperture mode is a good candidate to enhance the B.W% with sustaining gain and covers the complete band of 5G at 39 GHz.

The ACF approach, which has several modes of feeding an antenna, is used in the current work. This technology allows for the provision of feed through either width or length, and it is actually put into practice while the antenna is being designed. With this antenna, we priorities feed over width. A stack of two Rogers RT-Duroid 5880 PCB with an air gap of 0.035 mm and a height of 0.8 mm ($\epsilon_r = 2.2$) is used. The top side of the top layer has a ring radiator with a 4 mm outer radius, and the bottom is unmetalized. A plus-shaped slot is arranged on the upper side of the bottom layer, and the lower layer has a rectangular feed. The whole design setup is depicted in Fig. 1 and 2 respectively. The suggested antenna has a gain of 7.32 dBi and operates in the 36.84 GHz to 46.78 GHz spectrum, satisfying the 5G allotted band (mm-Wave-n260).

There are two sections to this work. Using Rogers-RT Duroid 5880 material, a microstrip patch antenna with an operating frequency of 38 GHz is created. Although there was wide bandwidth and good impedance matching in this area, the assigned bandwidth for this spectrum could not be reached. As this antenna spans about the frequency range

of 33 GHz to 39.5 GHz and has a peak gain of 8.1 dBi, its maximum S_{11} at 38 GHz is -43 dB. In several nations, this band is also reserved for 5G. Another component is the ACF method, which operates at 39 GHz with large bandwidth.

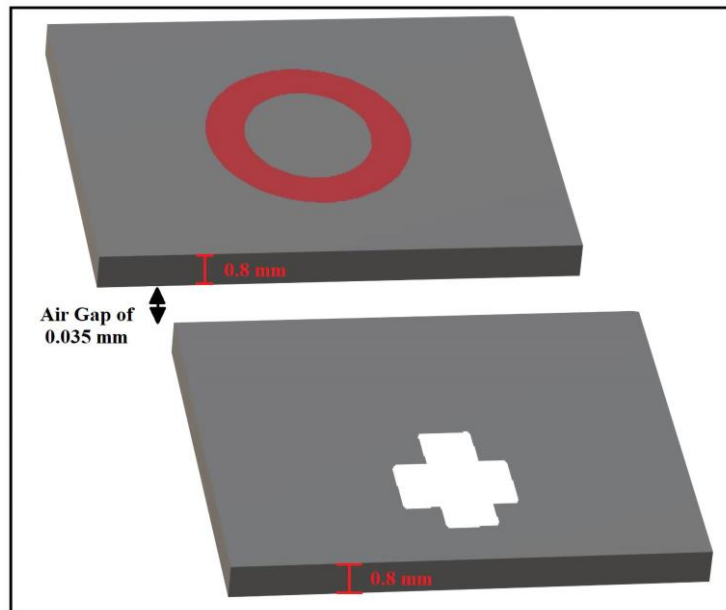


Fig.1. 3D- View of Aperture coupled feed antenna

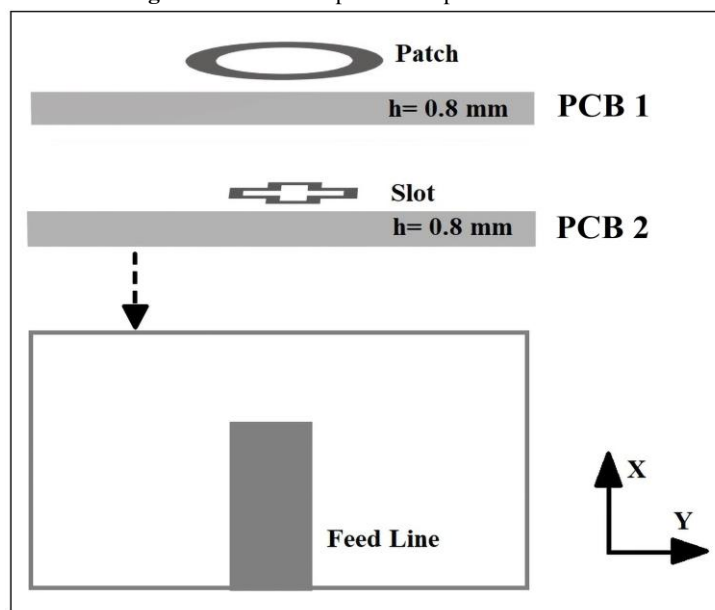


Fig.2. 2D- representation of ACF antenna

2 Design Approach

This section covers the design procedure for choosing a patch for the ring shape. Similar designs and dimensions have been used for ACF antenna and microstrip patch antenna. On a microstrip patch with the same dimension intended for ACF, the shape of the patch changes. For rectangular patch shape as dimensions of $7 \times 6 \times 0.8 \text{ mm}^3$, $7 \times 5.5 \times 0.8 \text{ mm}^3$, $6 \times 6 \times 0.8 \text{ mm}^3$, and $6 \times 7 \times 0.8 \text{ mm}^3$ are employed, however $7 \times 7 \times 0.8 \text{ mm}^3$ produces some of the good matching. Then we choose a hexagonal structure, however it does not achieve the required resonating band and it is incompatible. Then choose a circular shape with a radius between 3.5 mm to 2.5 mm. By using the radius value of 4 mm as the outer circle of the ring and the inner radius of the ring of 2 mm, the final patch as ring structure has decided because circular boundaries provide wide B.W, which is the main justification for choosing the patch structure as ring.

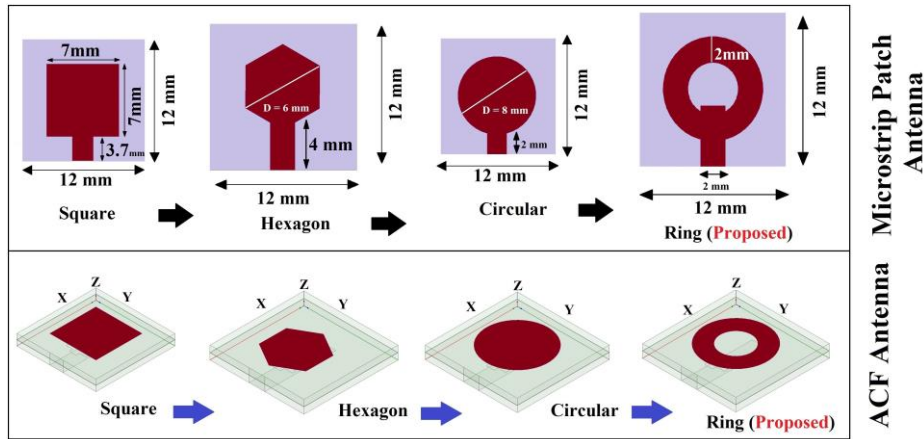


Fig. 3. Design approach for microstrip patch antenna and ACF antenna with various structure

Fig.3 provides a visual representation of both the microstrip patch and the ACF antenna. In Fig. 4 and 5, respectively, the comparative simulated response for both antenna and the suggested one is displayed. Square structures in ACF cases respond more quickly than rings, but only rings can provide the desired B.W. or wide B.W. The circular structure is another strong option for 5G communication because it operates at 38 GHz and provides good response. The smooth completion of the desired objective is seen throughout the better finding at the ring structure.

3 Microstrip Patch Antenna for 38 GHz

The operational frequency of a microstrip patch antenna (MSA) is 38 GHz, which is a licensed frequency for use in Mexico, the United States, and Japan for 5G communication [4-5]. Developed circular ring patch antenna with full ground the dimensions are presented in Fig.6.

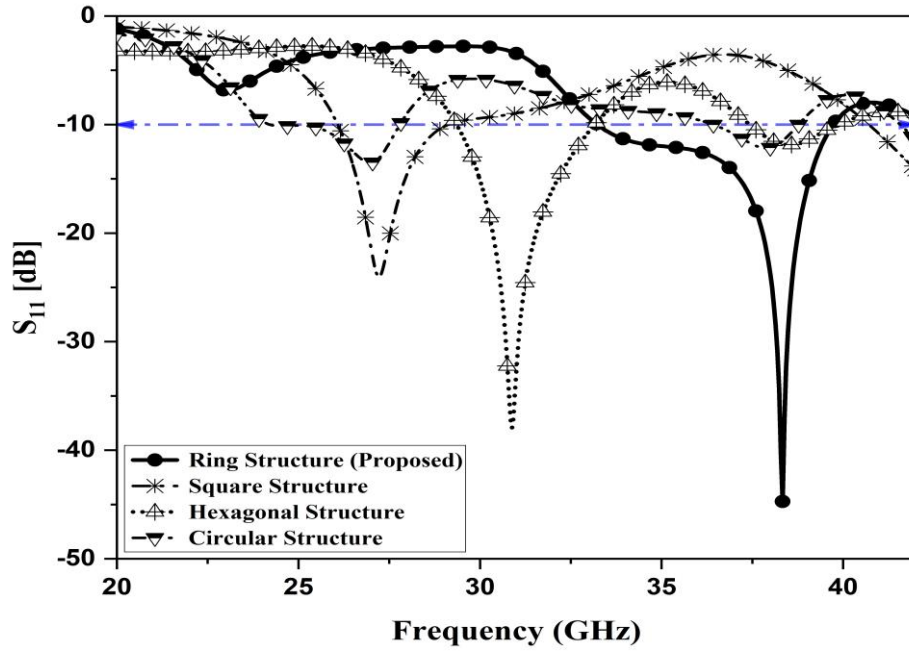


Fig. 4. Comparative response of various structure of Microstrip Patch Antenna

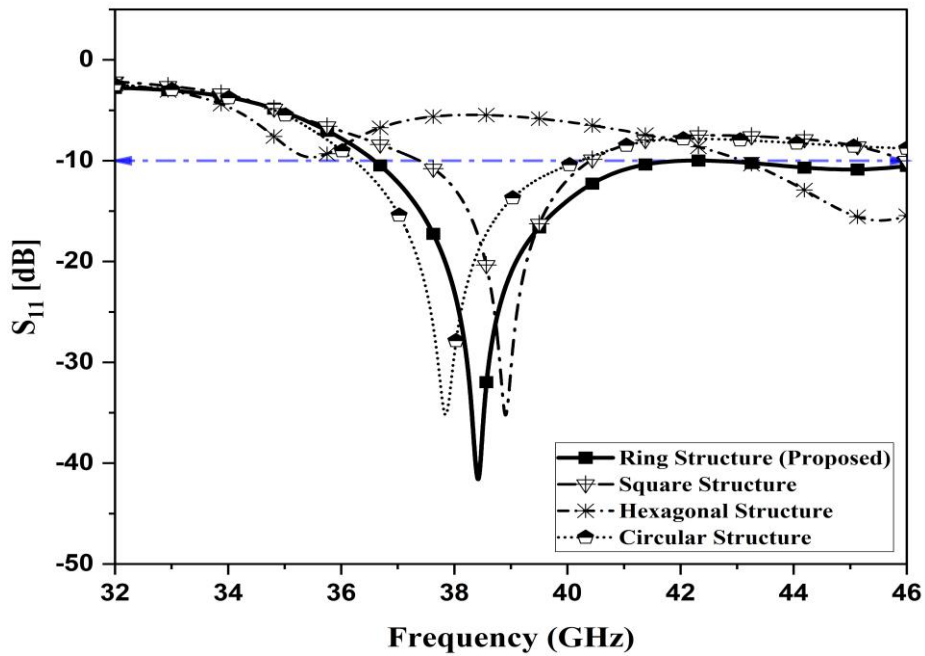


Fig. 5. Comparative response of various structure of Aperture Coupled Feed (ACF) Technique

Whereas its reflection coefficient, radiation patterns are shown in Fig 6 & 7 respectively. The feed line is of 4.7 mm in length with impedance value of 50Ω . The parametric study for circumference width of radiator is considered in sub section 3.1

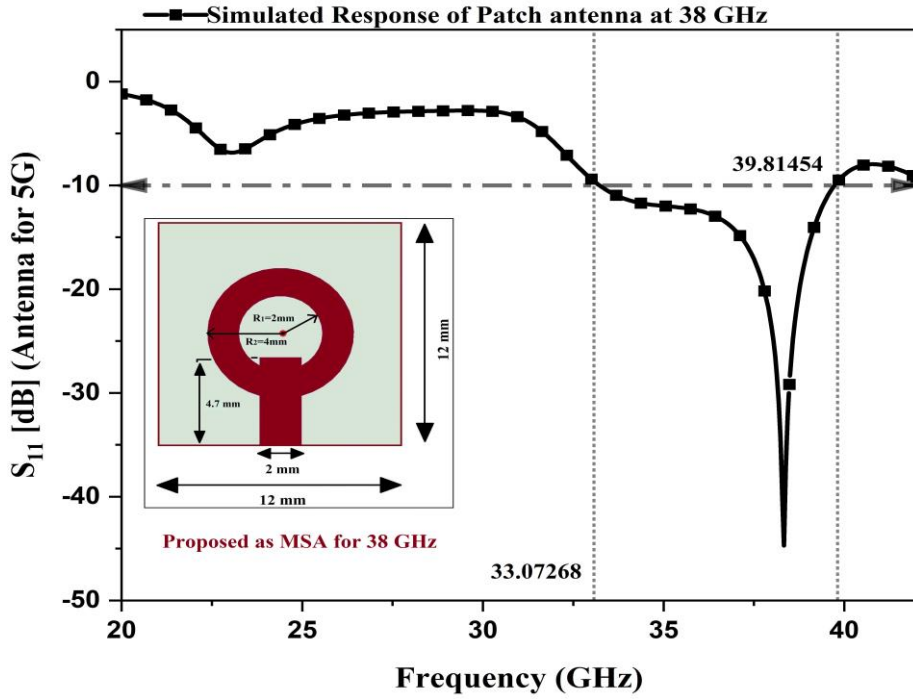


Fig. 6. Simulated response of S_{11} vs Freq. of patch antenna at 38 GHz with antenna's prototype

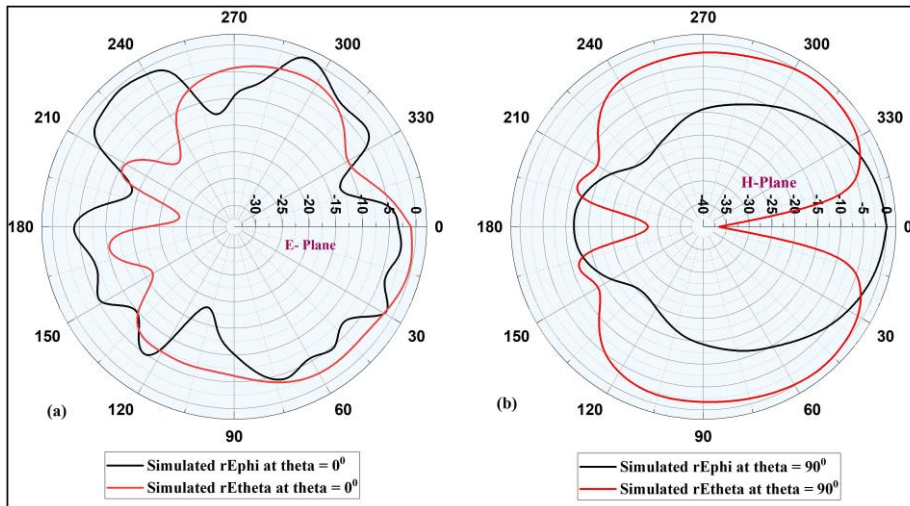


Fig. 7. Radiation pattern (a) E-plane (b) H-plane.

3.1 Parametric variations of circumference width of radiator

The antenna patch was specified by the radius difference between two circles, keeping the ground completely metallic. The simulated response that was observed as the gap was widened by 2.5, 3.0, and 3.2 mm is shown in Fig. 8.

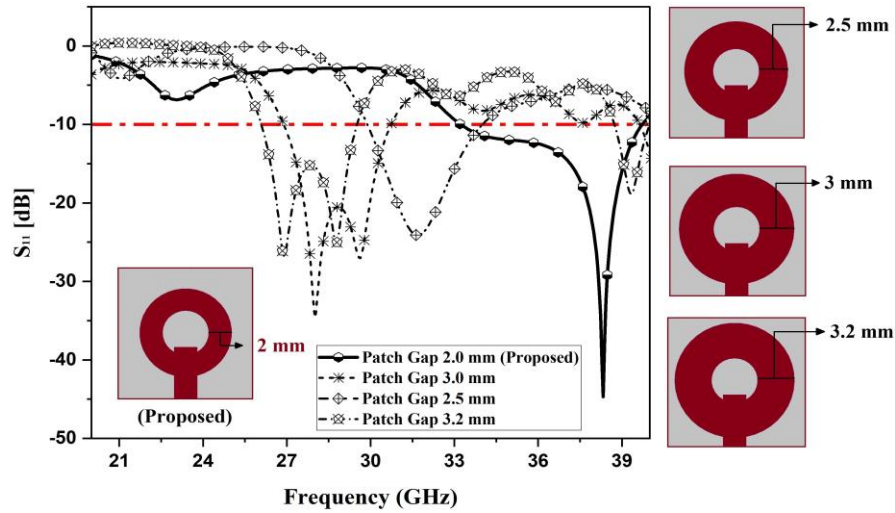


Fig. 8. Simulated response at higher value (variation of radius gap).

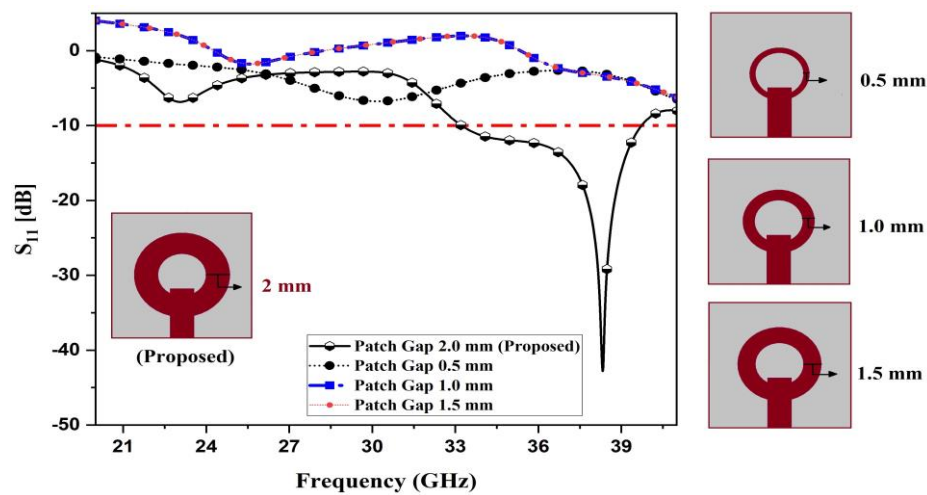


Fig. 9. Simulated response at lower value (variation of radius gap).

As the radius gap of the patch is increased, the resonant frequency shifts to the lower end. In this situation, such as when the antenna is 3.0 mm wide, it operates at 28 GHz and covers the 27–30 GHz frequency range, another 5G band. Similar to the higher

value of width, Fig. 9 shows the simulated response of scattering parameter at port 1 with frequency as per the variation of width of radiator towards lower value. The S_{11} value plot at lesser value variations at 1.0 mm and 1.5 mm, which have similar responses, extends from 0 to -14 dB at the right edge of the figure. In this scenario, every variation produces distinct outcomes with a minimum S_{11} value.

4 Aperture Coupled Feed Antenna Design

Using the stacking technique, an aperture coupled feed antenna, also known as an ACF antenna, is created with the antenna's feed coming through a slot. Two substrate-based antennas with either the same or differing relative permittivity values are used there. We employed two substrates with identical relative permittivity values for 39 GHz in this design. Because of its higher frequency applicability, this antenna is a candidate for global (world-wide) 5G communication. The values of the design parameter are displayed in Table 1. Fig. 10 displays the design antenna view with assigned parameter for both PCBs and Fig. 11 shows finished or fabricated PCBs and its development. Section 5 discusses the full analysis of ACF with various parameters, such as radiator width variation, feed length variation, and feed slot structure with different positions.

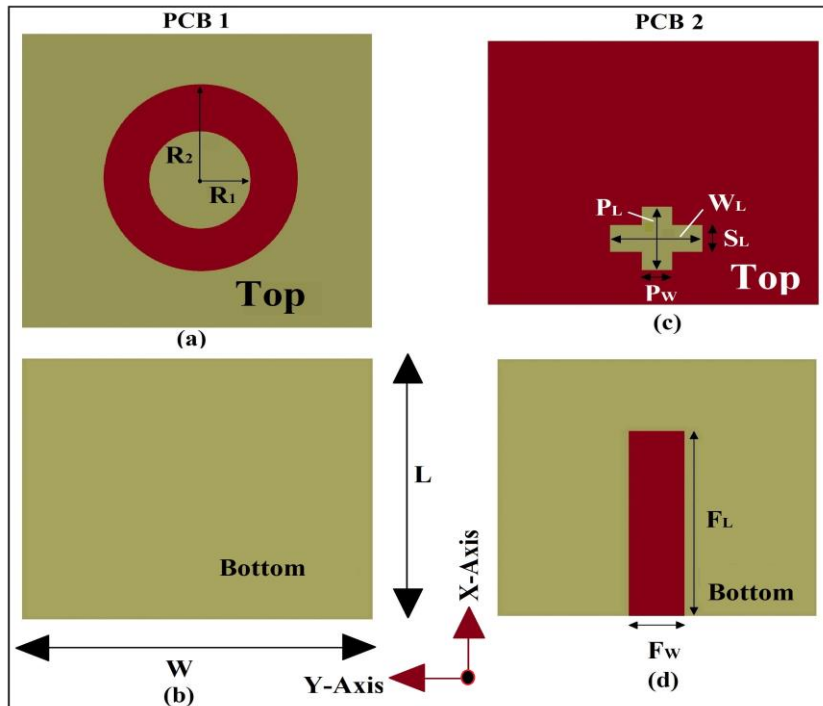
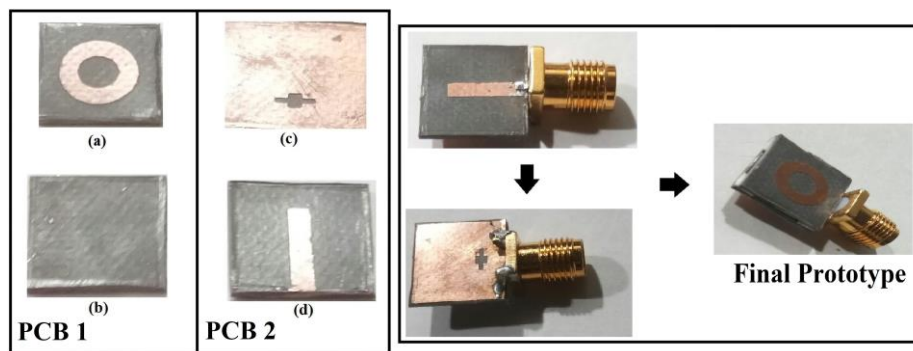


Fig.10. Antenna 2D view as (a) Top patch of PCB 1 (b) Ground view of PCB (c) Slot structure at top of PCB 2 (d) Feed line at PCB 2.

Table 1. Antenna's Parametric Value

Serial No.	Parameter	Value (ACF Antenna)
1	R_1 (Inner circle)	2 mm
2	R_2 (Outer circle)	4 mm
3	L (Length of ant.)	12 mm
4	W (Width of ant.)	12 mm
5	P_L (Length of Slot 1)	1.5 mm
6	P_W (Width of Slot 1)	1 mm
7	S_L (Length of Slot 2)	0.5 mm
8	W_L (Width of Slot 2)	3 mm

**Fig. 11.** Same view as top and ground with respect to substrate of fabricated antenna and steps to reach final prototype antenna

5 Parametric Analysis and Results of ACF Antenna

This section covers the parametric analysis of the antenna's various parametric analysis, including patch width, feed length, and slot creation. Several types of slot structures are used in this technique, and the effective slot is shown in the image above. With these terms, the study of the final reflection coefficient versus frequency result provides a clear picture of good impedance matching. To arrive at the outcome of the proposed antenna, we analyze S_{11} vs. frequency utilizing a number of instances.

5.1 Analysis of radiator width (Higher Value)

A variable is provided by the radius gap, which is defined as the inner radius less the outside radius. The gap for the proposed antenna would be 2 mm. The plot of S_{11} vs. Freq. for higher values of 2.5 mm, 3 mm, and 3.5 mm respectively is shown in Fig. 12 along with the schematic diagram of width variations of radiators. In this investigation, we found that the resonating frequency shifts to the lesser side and that the S_{11} value decreases in relation to the higher radius gap.

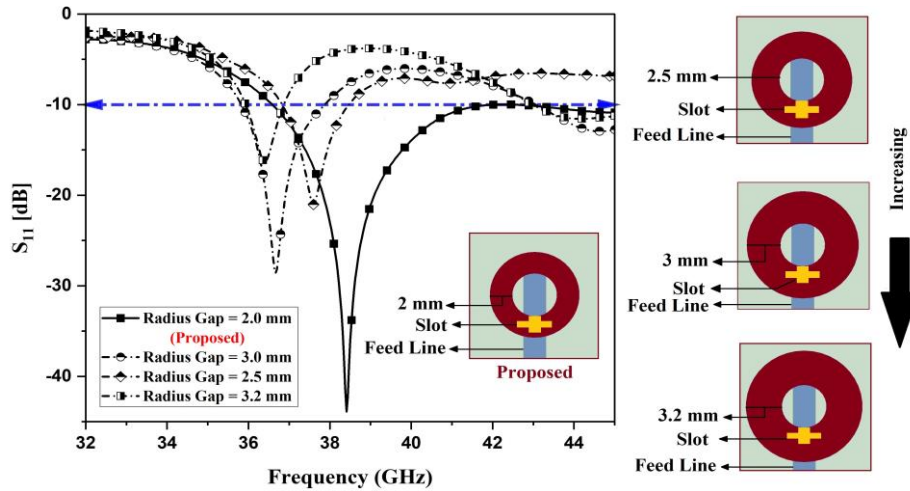


Fig.12. Simulated response of S_{11} vs Freq. for higher values.

5.2 Analysis of radiator width (Lower Value)

In this instance, we optimize with a lower value and monitor the output to analyze the return loss. The radius gap of the radiator with 1.5 mm, 1 mm, and 0.5 mm are chosen. Analysis of each value around the final proposed radius gap of 2 mm revealed that at this value the desired band with the highest S_{11} is seen. Fig. 13 displays the radius gap variation diagram and the simulated response of each antenna. Here, we determined that while matching grows worse as the radius gap increases toward the higher side, the resonating frequency also tends toward lower frequency. Due to the ACF approach, bandwidth is wider in each situation. In case of lower width radiator variation, the operating frequency moves at higher side with affective return loss.

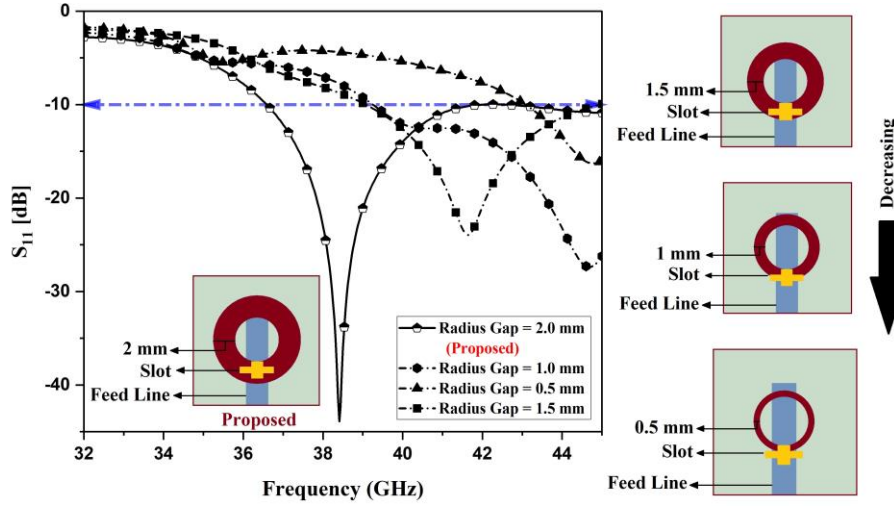


Fig.13. Simulated response of S_{11} vs Freq. for lower values.

5.3 Variations in Feed Line

Empirical formulae for feed length and width ($L_f = \lambda_l + \mathcal{E}_{eff}$ and $W_f = \mathcal{E}_{eff}$) where, $\lambda_l = C_l/F_0$ (C_l is speed of light and F_0 is operating frequency) are used to determine the length with 9.1 mm where width is of 2 mm. We analyze numerous feed length variations with respect to a maximum value greater than 9.1 mm and a minimum value lesser than the proposed value; the simulated response for the higher value is shown in Fig. 14. When the feed length is increased beyond the derived value, matching suffers and frequency response fluctuates. After analysis with maximum value by increasing the length with 1 mm the return loss and operating frequency is good at 9.1 mm (proposed). Fig.15 shows the simulated result for a feed line variation with smaller value with the difference of 1 mm respectively. Operating frequency starts increasing as feed line decreases. Before settling on this design, we experimented with several different options. We added a small slot with a meandering pattern to the feed line and used a small ring resonator as a slot structure to feed line. For better matching, we used the entire 12 mm feed length, but the ACF approach does not work with this. Feed line length will be provided up to the patch displayed on the top substrate. The matching feed line impedance value is of 50 ohms. Feed length could be calculated in terms of guided wavelength (λ_g) with regard to operating frequency. Single-layered microstrip patch antennas are quite effective with length of $\lambda_g/4$, $\lambda_g/2$ or λ_g but ACF's feed line does not calculated with these traditional formulae. The length from the port to slot or slot position can be of λ_g or $\lambda_g/4$ or $\lambda_g/2$ but in this case, we chosen $\lambda_g - \mathcal{E}_{eff}$. This shows while approaching towards the ACF antenna feed length and slot position must be accurate for wider B.W and perfect matching.

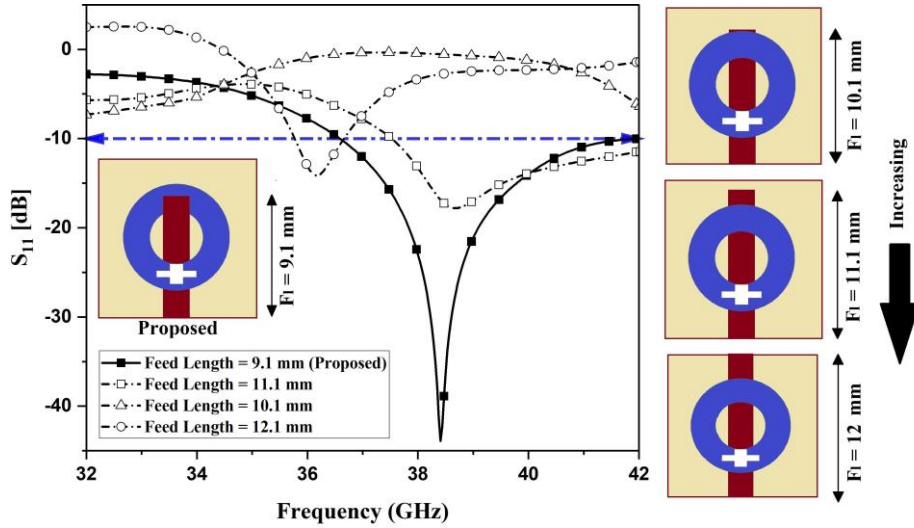


Fig. 14. Simulated response for feed length variation (Higher value).

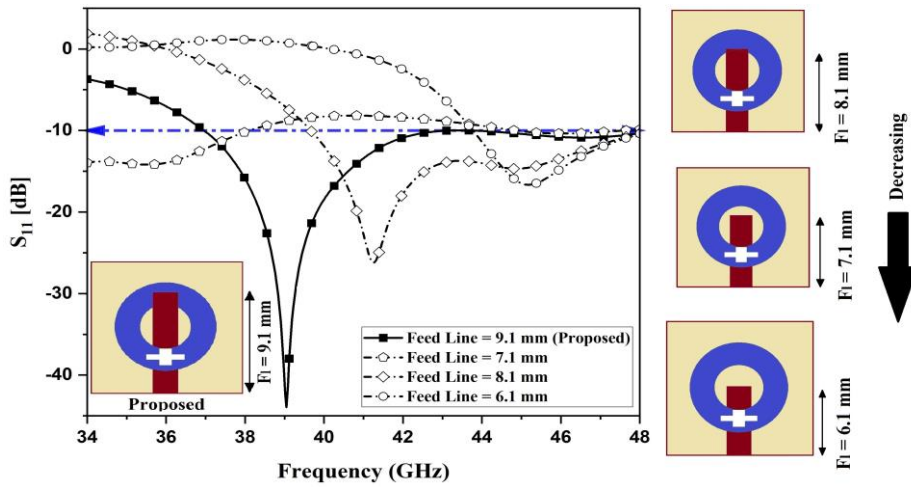


Fig. 15. Simulated response for feed length variation (lower value).

5.4 Variations in Slot or Selecting Slot Structure

Several slot structures are defined and analyzed as well as the slot used for power transmission to radiators. In this paper, we experimented with three distinct slot structures: circular, square, and rectangular. Additionally, the bottom, middle, and upper sides of the antenna's slots can also be changed. For the whole slot parameter analysis at these three distinct places, three (circular, square and rectangular) alternative size parameters have been used. Table 2 displays the slot structure's dimension as well as the position

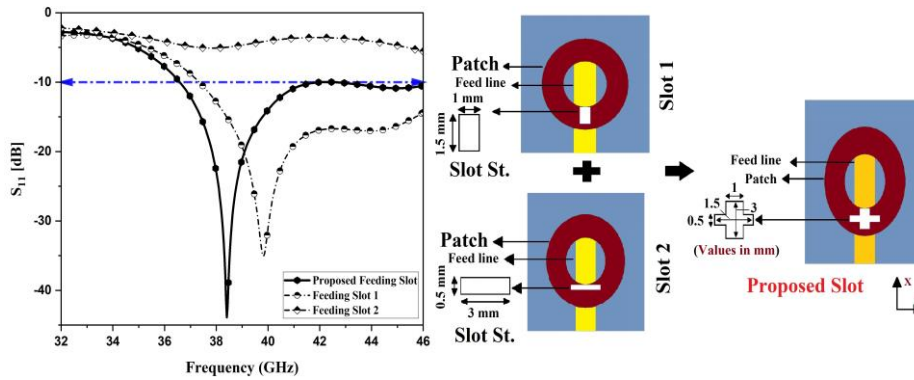


Fig.16. Response of slot structure (proposed) and approach of plus sign slot design.

Table 2. Slot structure along with different sizes, positions and findings.

Sl.no	Slot Position (X, Y, Z) mm	Shape of slot	Size of slot	Findings {Operating Frequency (O.F), S_{11} [dB]}
1.	Bottom (8,6,0.8)	Circular	Radius = 1.6 mm	O. F= 40 GHz, $ S_{11} = -13$ dB
2.	Bottom (8,6,0.8)	Circular	Radius = 2.2 mm	O. F= 34.5 GHz, $ S_{11} = -23$ dB
3.	Bottom (8,6,0.8)	Circular	Radius = 3.1 mm	O. F= 35 GHz & 43.2 GHz, $ S_{11} = -27$ & -43 dB
4.	Mid (6,6,0.8)	Circular	Radius = 1.2 mm	O. F= 37 GHz, $ S_{11} = -14.7$ dB
5.	Mid (6,6,0.8)	Circular	Radius = 2.5 mm	O. F= 39 GHz, $ S_{11} = -12$ dB (Larger B.W)
6.	Mid (6,6,0.8)	Circular	Radius = 4 mm	O. F= 36 GHz, $ S_{11} = -26$ dB
7.	Upper (3,6,0.8)	Circular	Radius = 1.4 mm	O. F= 36-38 GHz, $ S_{11} = -25$ dB
8.	Upper (3,6,0.8)	Circular	Radius = 2 mm	O. F= 37 GHz, $ S_{11} = -14$ dB
9.	Upper (3,6,0.8)	Circular	Radius = 3 mm	O. F= 39 GHz, $ S_{11} = -24$ dB (Larger B.W)
10.	Bottom (8,5,0.8)	Square	Size = 2×2 mm ²	O. F= Beyond Objective, $ S_{11} = NA$
11.	Bottom (7.75, 4.75,0.8)	Square	Size = 2.5×2.5 mm ²	O. F= 45 GHz, $ S_{11} = -25$ dB
12.	Bottom (7.5,4.5,0.8)	Square	Size = 3×3 mm ²	O. F= 43 GHz, $ S_{11} = -12$ dB
13.	Mid (5.75,4.75,0.8)	Square	Size = 2.5×2.5 mm ²	O. F= 45 GHz, $ S_{11} = -20$ dB
14.	Mid (4.75,3.75,0.8)	Square	Size = 3.5×3.5 mm ²	O. F= 39 GHz, $ S_{11} = -11$ dB
15.	Mid (4.25,4.25,0.8)	Square	Size = 4.5×4.5 mm ²	O. F= 39 GHz, $ S_{11} = -9.6$ dB
16.	Upper (3.5,5,0.8)	Square	Size = 2×2 mm ²	O. F= 37 GHz, $ S_{11} = -11$ dB
17.	Upper (2,4.45,0.8)	Square	Size = 3×3 mm ²	O. F= 37.2 GHz, $ S_{11} = -9.3$ dB
18.	Upper (2.5,4,0.8)	Square	Size = 4×4 mm ²	O. F= Irregular Pattern, $ S_{11} = NA$
19.	Bottom (9,4.5,0.8)	Rectangular	Size = 1×3 mm ²	O. F= 36.6 GHz, $ S_{11} = -13.8$ dB
20.	Bottom (8,5,4,5,0.8)	Rectangular	Size = 2×3 mm ²	O. F= 36 GHz, $ S_{11} = -34$ dB
21.	Bottom (7,5,5,0,8)	Rectangular	Size = 3×2 mm ²	O. F= 45 GHz, $ S_{11} = -20$ dB
22.	Mid (6,4,0.8)	Rectangular	Size = 1×4 mm ²	O. F= 45 GHz, $ S_{11} = -34$ dB
23.	Mid (5,75, 4,5, 0,8)	Rectangular	Size = 1.5×3 mm ²	O. F= Beyond 46 GHz, $ S_{11} = -NA$
24.	Mid (5,5,4,0.8)	Rectangular	Size = 2×4 mm ²	O. F= 46 GHz, $ S_{11} = -20$ dB
25.	Upper (1,75,4,0,8)	Rectangular	Size = 2.5×4 mm ²	O. F= 38 GHz, $ S_{11} = -23.2$ dB
26.	Upper (1,5,4,0,8)	Rectangular	Size = 3×4 mm ²	O. F= 37 GHz, $ S_{11} = -17$ dB
27.	Upper (1,4,75,0,8)	Rectangular	Size = 4×2.5 mm ²	O. F= 36 GHz, $ S_{11} = -7$ dB

and results based on simulated response as operating frequency and return loss. Fig. 17 displays the responses of each structure, which are grouped into three places labelled bottom, middle, and top, respectively. The rectangular slot of two separate structures is

used to complete the slot structure after it was discovered in this analysis that the slot should remain on the bottom side and perform better than other structures. Using two rectangular slots of different sizes, combining them, and maintaining the bottom end, as illustrated in Fig. 16. Addition sign (+) slot is suggested, and another structure at the bottom end gives the appropriate working frequency, supporting the concept of placing it there. In Fig. 16, the simulated response for both rectangular slots and the suggested slot are also displayed.

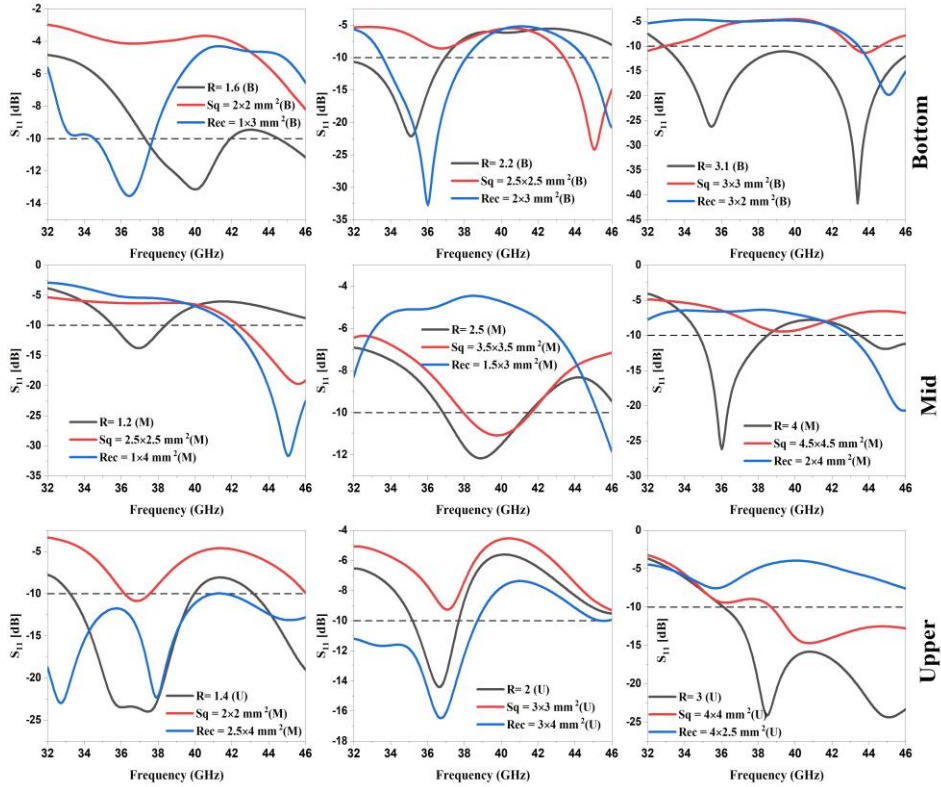


Fig. 17. Simulated response of different slots at multiple positions (Bottom, Mid, Upper)

6 Experimental Setup, Results and Discussion

This section includes a visual illustration of the experimental setup for measuring the antenna parameter and a discussion of the findings. The final antenna prototype is shown in Fig. 18 where (a) and (b) show the antenna's picture at various angles from the front and 3D views, respectively, after merging PCB₁ and PCB₂ with an air gap of 0.035mm. Rest displays the top, middle, bottom and side view of the ACF antenna. The

antenna is then placed in front of the VNA for testing. To accomplish the response at the VNA for calibration, we employ a matched SMA connector. The measuring setup and VNA results are displayed in Fig. 19. The measured S_{11} value of -35.89 dB covers nearly the entire range allotted for this frequency globally or worldwide with wide B.W.

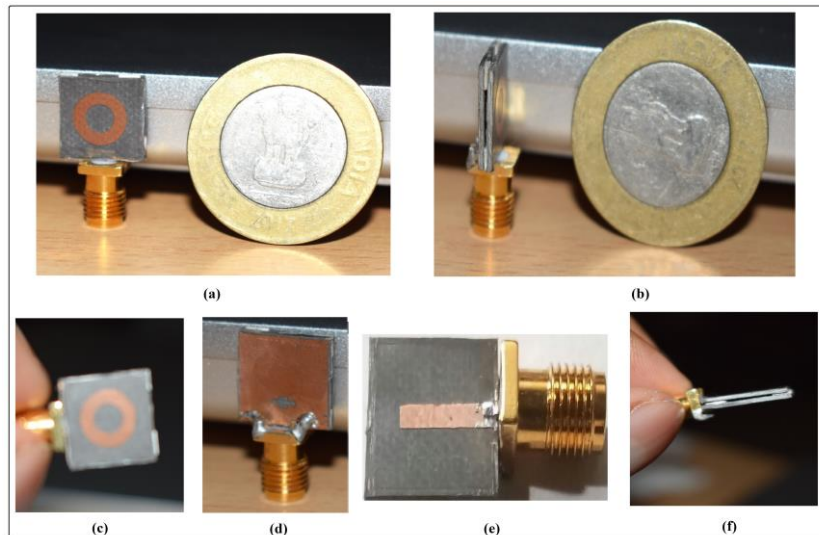


Fig. 18. Fabricated antenna (a) Front view (b) 3D view (c) Top patch view (d) Middle slot view (e) Bottom ground view (f) Side view.

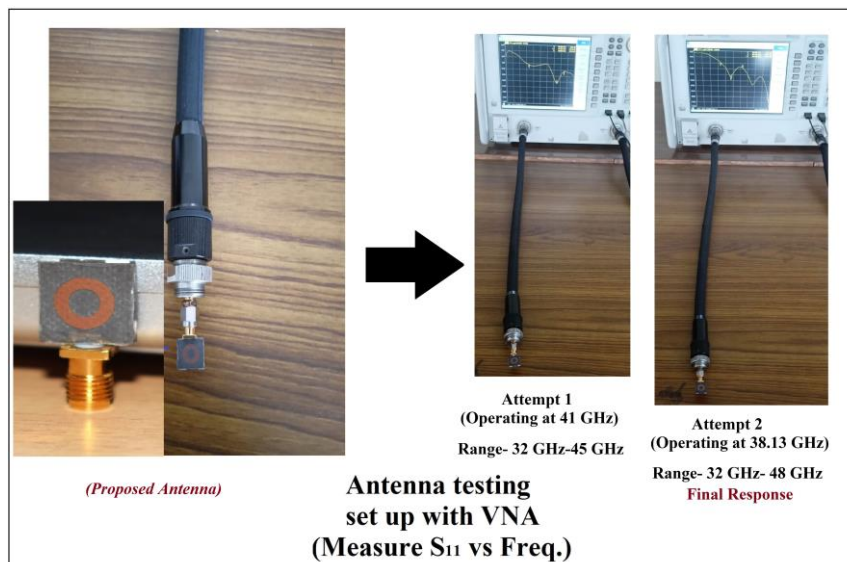


Fig.19. Experimental set up of antenna with VNA for measuring the response of reflection coefficient vs. frequency response.

As demonstrated in Fig. 20's measured and simulated response of reflection coefficient and frequency. With the intended bandwidth, the simulated value of $S_{11} = -40.40$ dB and gain of 7.32 dBi. Fig. 21 depicts the set-up in an anechoic chamber with an antenna for measuring the radiation pattern, with (a) the antenna directed at the sending end and

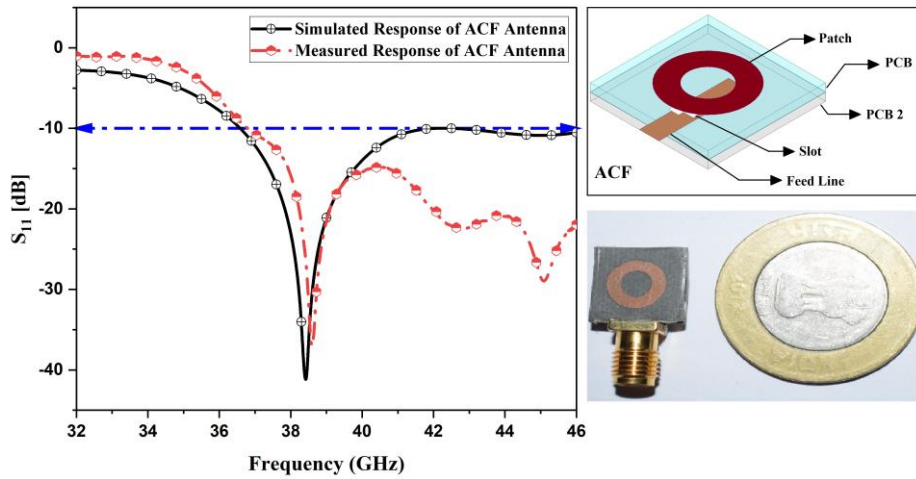


Fig. 20. Measured and simulated response of S_{11} and frequency response

(b) the antenna oriented at the receiving end. Fig. 22 shows the pattern produced in the measured and simulated cases using the E- and H-planes, respectively. If the target angle is 0 degrees or 90 degrees for phi or theta, respectively, the measured and simulated data is normalized by dividing each case by the maximum value.

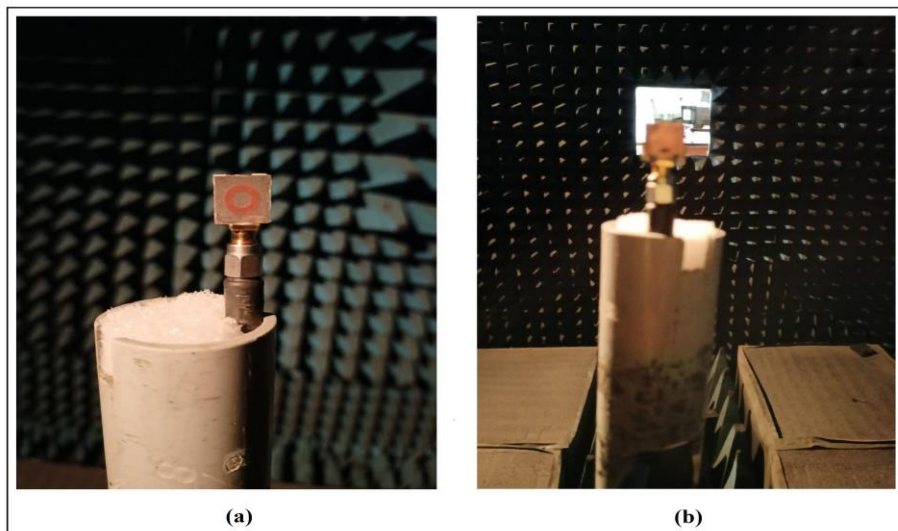


Fig. 21. Antenna measuring set up for beam pattern measuring of ACF antenna (a), (b)

The simulated pattern is omnidirectional even for $\theta = 0^\circ$ poses about to directional at two different angles, as in the E-plane plot for $\phi = 0^\circ$ measured as well as simulated pattern. The antenna for the H-plane also displays a directional plot at the 0° angle at $\phi = 90^\circ$ and $\theta = 90^\circ$.

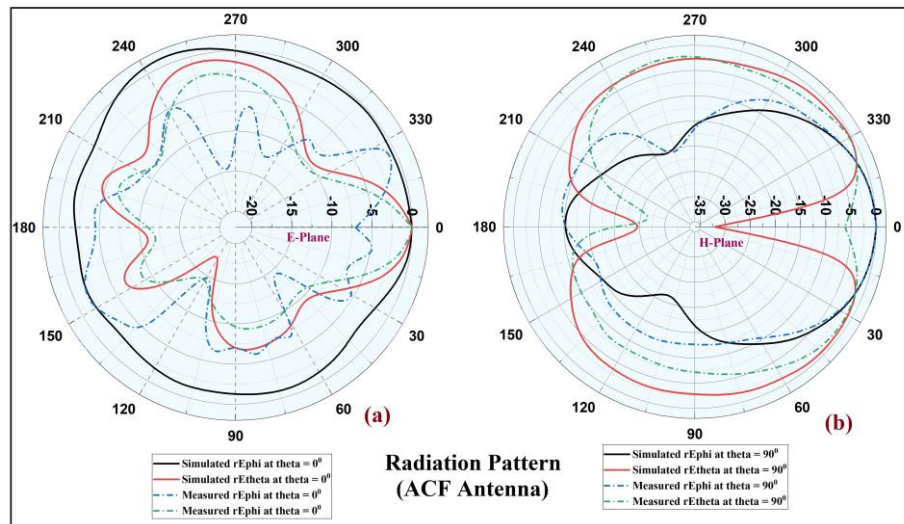


Fig. 22. Radiation pattern (a) Simulated and measured E-plane (b) Simulated and measured H-plane

Another factor that characterizes the effectiveness of power transmitted or provided to conducting elements is voltage standing wave ratio (VSWR). The ideal efficiency is determined when full power is delivered to the load element. The recommended range

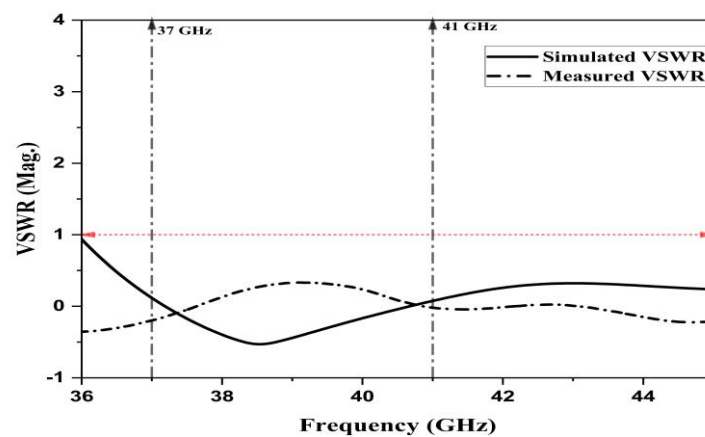


Fig. 23. Simulated and measured response of VSWR (Mag.)

of VSWR is less than 1, while a number between 1.5 and 2 is considered slightly acceptable. Fig. 23 displays the simulated and measured VSWR response to standardize the performance of the antenna. At $F_c = 38.40$ GHz, the observed value is 0.2, while the simulated value is -0.6. In simulated and measured cases, the VSWR is acceptable and is less than 1. Fig. 24 (a) and Fig. 24 (b) displays the current density field plot of in ampere per meter (A/m) with value of 38 A/m and the electric field (E) plot in amperes per meter (A/m) with max value of 5046 A/m respectively. The patch distribution or flow of these quantities provides information regarding the rate of electron flow relative to the specified structure.

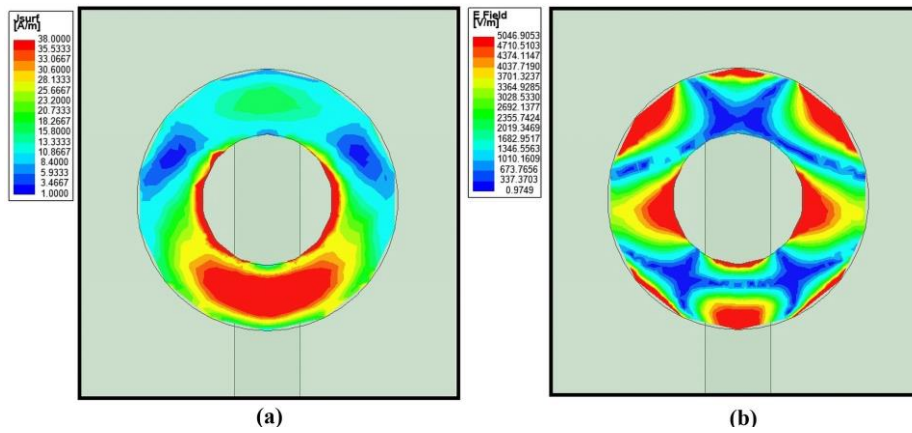


Fig. 24. Field plot (a) Current density (J) plot (A/m) (b) Electric field plot (v/m).

We examine a few papers' analyses and literature reviews and contrast them with our own work. For low frequency applications, it is preferable to employ the designed antenna technique. Numerous switching, stacking, and arraying techniques are employed in 5G applications. Comparative table (Table 3) displays the comparison of own work with the previous work.

7 Conclusion

The microstrip patch antenna is initially obtained and analyzed at 38 GHz, and subsequently it is successfully obtained and tested in its stacked version at 39 GHz. A stack antenna is chosen using the ACF approach, and both PCBs are made of RT Duroid 5880 ($\epsilon_r = 2.2$). Power is provided to the patch through the slot, causing it to excite PCB₁ while PCB₂ receives the feed. By connecting the antenna, the reflection coefficient was calculated to be -35.89 dB in measurement and -40.40 dB in simulation. This antenna's B.W% is 25.9% and its highest gain is 7.32 dBi. The Size of antenna is $12 \times 12 \times 1.635$ mm³ where PCB₁ height is 0.8 mm, PCB₂ height is 0.8 mm and 0.035

mm is air gap. Applicable globally for 5G communication with wider bandwidth of 9.1 GHz. This proposed antenna is used in wireless communication for 5G communication globally with maximum data transmission without delay.

Table 3. Comparison table of proposed work with past work

Ref.	Antenna Technique	Op. freq. / B. W	Design Constraint	Substrate	Gain	Others Param.
[6]	C structured 2x2 MIMO	28/38 GHz	10x10x0.254mm ³	Rogers RT Duroid ($\epsilon_r=2.2$)	7.4 dBi/8.56 dBi	NA
[7]	Reconfigurable by using PIN Diode	38/28 GHz	PCB h = 0.506 mm	Rogers RT Duroid ($\epsilon_r=2.2$)	NA	$S_{11} = -32.3$ dB/ $S_{11} = -42.1$ dB
[8]	Single layered to multi layered antenna	28/38.5GHz	Array (4 element) of single layered antenna	Multiple (flexible)	4.8 dBi /4.6 dBi	NA
[9]	Hook shaped aperture coupled feed antenna	2.8–3.81 GHz	28 ×24 ×2 mm ³	FR4 ($\epsilon_r=4.4$)	4.08 dBi	Return loss % =29.10 %
[10]	Aperture coupled feed (Two Port)	3.3–3.8 GHz	50x50x12.5 mm ³	PCB 1 = FR4 ($\epsilon_r=4.4$); h= 1 mm PCB 2 = Roger RO4003 ($\epsilon_r=3.38$); h=0.508 mm	7.9 dBi- 8.5 dBi	VSWR is <1.5
[11]	Air-filled Substrate Integrated Waveguide (AF-SIW) with stack	24.25-29.5 GHz	26x26x1.8 mm ³ (LxBxH)	PCB 1 = RO4350B PCB 2 = FR4 ($\epsilon_r=4.4$) PCB 3 = RO350B	10.1 dBi	B.W % = 26.8 %
[25]	Stack Antenna	27.5-28.5 GHz	Substrate height = 0.508 mm	Tectonic TL4	21 dBi	B.W % = 9.8 %
[26]	Printed RGW Aperture	30 GHz	Substrate height = 0.5 mm	RO3003 with $\epsilon_r = 3$	13.5 dBi	Radiation Efficiency = 84%
[28]	Graphene Array Antenna	13.8-15.15 GHz	Substrate thickness range Kapton – 0.075 mm A4 Page- 0.05 mm Rogers RT Duroid - 0.254 mm	Kapton ($\epsilon_r=3.5$) A4 Page ($\epsilon_r=3.2$) RT Duroid ($\epsilon_r=2.2$)	7 dBi	B.W varied based on different material
Prop.	Aperture coupled feed antenna	39 GHz (36.84 – 46.78 GHz)	12x12x1.635 mm³	PCB1 =RO5880 ($\epsilon_r=2.2$) PCB 2=RO5880 ($\epsilon_r=2.2$)	7.32 dBi	B.W %= 25.68 % S₁₁ = -40.4 dB

Acknowledgement / Funding

NA- Not Available / No Funding

Competing Interests

The author(s) declare none.

References

1. Chaudhary, S., & Kansal, A. (2021). Triband Millimeter-wave Antenna for 5G Mobile Communications. *Iranian Journal of Science and Technology, Transactions of Electrical Engineering*, 45, 1217-1226.
2. Dzagbletey, P. A., & Chung, J. Y. (2023). Conductive Ink Printed Fabric Antenna with Aperture Feeding Technique. *Applied Sciences*, 13(5), 2902.
3. Pigeon, M., Delaveaud, C., Rudant, L., & Belmkaddem, K. (2014). Miniature directive antennas. *International Journal of Microwave and Wireless Technologies*, 6(1), 45-50.
4. Dash, S. K. K., Cheng, Q. S., & Khan, T. (2021). A superstrate loaded aperture coupled dual-band circularly polarized dielectric resonator antenna for X-band communications. *International Journal of Microwave and Wireless Technologies*, 13(8), 867-874.
5. 5G Americas, 3GPP 5G NR NSA specification and wireless 20/20, December 2018.
6. Chaudhary, S., & Kansal, A. (2022). Compact high gain 28, 38 GHz antenna for 5G communication. *International Journal of Electronics*, 1-21.
7. Shereen, M. K., & Khattak, M. I. (2022). A hybrid reconfigurability structure for a novel 5G monopole antenna for future mobile communications at 28/38 GHz. *Arabian Journal for Science and Engineering*, 47(3), 2745-2753.
8. Hwang, I. J., Oh, J. I., Jo, H. W., Kim, K. S., Yu, J. W., & Lee, D. J. (2021). 28 GHz and 38 GHz dual-band vertically stacked dipole antennas on flexible liquid crystal polymer substrates for millimeter-wave 5G cellular handsets. *IEEE Transactions on Antennas and Propagation*, 70(5), 3223-3236.
9. Swetha, R., & Anjaneyulu, L. (2021). Novel design and characterization of wide band hook shaped aperture coupled circularly polarized antenna for 5G application. *Prog. Electro-magn. Res. C*, 113, 161-175.
10. Cam Ha Le Thi; Son Xuat Ta; Xuan Quyen Nguyen; Khac Kiem Nguyen; Chien Dao-Ngoc; (2021). Design of compact broadband <sc>dual-polarized</sc> antenna for <sc>5G</sc> applications. *International Journal of RF and Microwave Computer-Aided Engineering*, (), -. doi:10.1002/mmce.22615
11. de Paula, I. L., Lemey, S., Bosman, D., Van den Brande, Q., Caytan, O., Lambrecht, J., ... & Rogier, H. (2020). Cost-effective high-performance air-filled SIW antenna array for the global 5G 26 GHz and 28 GHz bands. *IEEE Antennas and Wireless Propagation Letters*, 20(2), 194-198.
12. Van den Brande, Q., Lemey, S., Vanfleteren, J., & Rogier, H. (2018). Highly efficient impulse-radio ultra-wideband cavity-backed slot antenna in stacked air-filled substrate integrated waveguide technology. *IEEE Transactions on Antennas and Propagation*, 66(5), 2199-2209.
13. Mohamed, I. M., & Sebak, A. R. (2019). 60 GHz 2-D scanning multibeam cavity-backed patch array fed by compact SIW beamforming network for 5G applications. *IEEE Transactions on Antennas and Propagation*, 67(4), 2320-2331.
14. Kapusuz, K. Y., Lemey, S., & Rogier, H. (2019, October). Dual-polarized 28-GHz air-filled SIW phased antenna array for next-generation cellular systems. In *2019 IEEE International Symposium on Phased Array System & Technology (PAST)* (pp. 1-6). IEEE.
15. Belenguer, A., Esteban, H., & Boria, V. E. (2014). Novel empty substrate integrated waveguide for high-performance microwave integrated circuits. *IEEE transactions on microwave*

- theory and techniques*, 62(4), 832-839.
16. Parment, F., Ghiotto, A., Vuong, T. P., Duchamp, J. M., & Wu, K. (2015). Air-filled substrate integrated waveguide for low-loss and high power-handling millimeter-wave substrate integrated circuits. *IEEE Transactions on Microwave Theory and Techniques*, 63(4), 1228-1238.
 17. Parment, F., Ghiotto, A., Vuong, T. P., Duchamp, J. M., & Wu, K. (2016). Double dielectric slab-loaded air-filled SIW phase shifters for high-performance millimeter-wave integration. *IEEE Transactions on Microwave Theory and Techniques*, 64(9), 2833-2842.
 18. Parment, F., Ghiotto, A., Vuong, T. P., Duchamp, J. M., & Wu, K. (2017). Ka-band compact and high-performance bandpass filter based on multilayer air-filled SIW. *Electronics Letters*, 53(7), 486-488.
 19. Morro, J. V., Rodríguez, A., Belenguer, A., Esteban, H., & Boria, V. (2016). Multilevel transition in empty substrate integrated waveguide. *Electronics Letters*, 52(18), 1543-1544.
 20. Van den Brande, Q., Lemey, S., Cuyvers, S., Poelman, S., De Brabander, L., Caytan, O., ... & Rogier, H. (2019). A hybrid integration strategy for compact, broadband, and highly efficient millimeter-wave on-chip antennas. *IEEE Antennas and Wireless Propagation Letters*, 18(11), 2424-2428.
 21. Li, Y., & Luk, K. M. (2014). Low-cost high-gain and broadband substrate-integrated-waveguide-fed patch antenna array for 60-GHz band. *IEEE Transactions on Antennas and Propagation*, 62(11), 5531-5538.
 22. Li, Y., & Luk, K. M. (2015). 60-GHz substrate integrated waveguide fed cavity-backed aperture-coupled microstrip patch antenna arrays. *IEEE Transactions on Antennas and Propagation*, 63(3), 1075-1085.
 23. Parment, F., Ghiotto, A., Vuong, T. P., Duchamp, J. M., & Wu, K. (2017). Millimetre-wave air-filled substrate integrated waveguide slot array antenna. *Electronics Letters*, 53(11), 704-706.
 24. Qi, Z., Li, X., Xiao, J., & Zhu, H. (2019). Low-cost empty substrate integrated waveguide slot arrays for millimeter-wave applications. *IEEE Antennas and Wireless Propagation Letters*, 18(5), 1021-1025.
 25. Diawuo, H. A., & Jung, Y. B. (2018). Broadband proximity-coupled microstrip planar antenna array for 5G cellular applications. *IEEE Antennas and Wireless Propagation Letters*, 17(7), 1286-1290.
 26. Ali, M. M. M., & Sebak, A. (2019). Printed RGW circularly polarized differential feeding antenna array for 5G communications. *IEEE Transactions on Antennas and Propagation*, 67(5), 3151-3160.
 27. Tighezza, M., Rahim, S. K. A., & Islam, M. T. (2018). Flexible wideband antenna for 5G applications. *Microwave and Optical Technology Letters*, 60(1), 38-44.
 28. Sa'don, Siti Nor Hafizah, Muhammad Ramlee Kamarudin, Fauzan Ahmad, Muzammil Jusoh, and Huda A. Majid. "Graphene array antenna for 5G applications." *Applied Physics A* 123 (2017): 1-4.
 29. Li, T., & Chen, Z. N. (2019). Shared-surface dual-band antenna for 5G applications. *IEEE Transactions on Antennas and Propagation*, 68(2), 1128-1133.
 30. Wang, W., Wu, Y., Wang, W., & Yang, Y. (2020). Isolation enhancement in dual-band monopole antenna for 5G applications. *IEEE Transactions on Circuits and Systems II: Express Briefs*, 68(6), 1867-1871.
 31. Jafarabadi, A., & Forooghi, K. (2019). Design of a Novel Feeding Network for a Subarrayed Monopulse Linear Array Antenna. *Iranian Journal of Science and Technology, Transactions of Electrical Engineering*, 43, 51-59.

Supplementary Files

This is a list of supplementary files associated with this preprint. Click to download.

- [AuthorDetails.pdf](#)